Carbon 111 (2017) 764–773

Contents lists available at ScienceDirect

Carbon

journal homepage: www.elsevier.com/locate/carbon

Morphology and texture of spheroidized natural and synthetic graphites

Manuel Mundszinger [a], Sarvenaz Farsi [b], Manfred Rapp [b], Ute Golla-Schindler [a, 1], Ute Kaiser [a, *], Mario Wachtler [b, **]

[a] Electron Microscopy Group of Materials Science, Central Facility for Electron Microscopy, University Ulm, Albert-Einstein-Allee 11, 89081 Ulm, Germany
[b] ZSW –Zentrum für Sonnenenergie- und Wasserstoff-Forschung Baden-Württemberg, Helmholtzstraße 8, 89081 Ulm, Germany

ARTICLE INFO

Article history:
Received 28 June 2016
Received in revised form
20 October 2016
Accepted 22 October 2016
Available online 24 October 2016

ABSTRACT

The electrochemical performance of mechanically spheroidized natural and synthetic graphite particles is significantly influenced by the type of spheroidization process used and the applied conditions. In order to guarantee a consistent and high material quality, spherical graphite particles have to be carefully benchmarked before use. Three spherical natural graphites and three spheroidized synthetic graphites are characterized using several physical analysis methods. A special focus is laid on the internal morphology and texture, which has been studied by scanning electron microscopy (SEM) – focused ion beam (FIB) cross-sections and tomography. For the spheroidized natural graphites under investigation this method indicates a volume of closed pores in the range of 4–5% and of open pores of 0.5% or less of the total particle volume. With increasing energy impact during the spheroidization process the open porosity increases and the closed porosity decreases.

1. Introduction

Natural graphite (NG) is the dominant anode material for lithium ion batteries (LIBs) today, with a market share of approximately 55% [1]. With the continuous growth of portable, automotive and other applications the total LIB market is expected to more than double within the next 5–10 years. In view of this growth scenario, some prognoses predict severe supply bottlenecks of NG. Furthermore, the NG sources are geographically strongly concentrated today, which poses an immanent risk to supply security [2]. In principle, the increasing demand for graphite as LIB anode material can be met by synthetic graphite (SG), for which an upscaling of the production capacity is possible with economically justifiable effort within short time. Nonetheless, there are strong activities to develop new sources of NG for LIBs, especially in Canada and South-East Africa [3].

During mining and the following processing steps, NG is, due to its highly anisotropic structure, obtained in the form of flat flakes with a large aspect ratio. In order for NG to be used for LIBs, these pristine flakes are usually mechanically turned into spherical shapes by a process called “spheroidization”, and coated with a thin film of amorphous carbon. As a result of this processing, problems concerning graphite exfoliation due to electrolyte solvent co-intercalation during lithium intercalation are alleviated and the surface area of the spherical material is reduced, leading to a decreased irreversible capacity in the first charge/discharge cycle [3,4].

Without spheroidization, the NG flakes have the tendency to orient themselves in parallel to the current collector during electrode preparation. This orientation slows down the Li^+ intercalation and de-intercalation process, as the lithium ions cannot enter the graphite crystal through its “basal plane surface” which is oriented towards the electrolyte, but have to migrate all the way around the flakes to the “prismatic surface planes” [5,6]. (The “basal plane surfaces” are the surfaces which are parallel to the crystallographic (001) plane of the hexagonal graphite lattice and to the single graphene layers, and the “prismatic surface planes” are the surfaces perpendicular to them.)

By mechanical treatment (such as milling or spheroidizing) of NG flakes, numerous crystal defects arise and the sizes of the former extended crystals are decreased, as described for example

* Corresponding author.
** Corresponding author.
E-mail addresses: ute.kaiser@uni-ulm.de (U. Kaiser), mario.wachtler@zsw-bw.de (M. Wachtler).
[1] Present address: Material Research Institute Aalen, Aalen University, Beethovenstraße 1, 73430 Aalen, Germany.

http://dx.doi.org/10.1016/j.carbon.2016.10.060
0008-6223/

by X-ray diffraction measurements [7], transmission electron microscopy investigations [8] or Raman spectroscopic analyses [6]. Accordingly, mechanically spheroidized NG particles with a suitable size (the industrial standard for LIBs is around 8–30 μm [9]) open access for fast and extensive lithium intercalation into small crystal layers, independently of the orientation of the particle on the current collector, thus enhancing the electrochemical performance of the material [6].

Another advantage of spheroidizing NG flakes is an increase of the powder tap density [10], which not only improves the packing density and thus the volumetric capacity of the graphite when used as anode active material in LIBs, but also has a positive influence on the discharge rate capability [11].

The mechanical spheroidization of various materials (toner material, calcium carbonate and copper), but not graphite, was described in 1994 by M. Otani et al. [12] using a rotational dry impact blending mill in lab-scale. Since then this method to modify the shape of particles was investigated for other materials, like, for example, stainless steel [13], but also for mixtures of materials, like polyethylene and hydroxyapatite [14].

One of the first patents describing spherical NG was filed in 1998 by S. Kubota et al. (Kansai Netsukagaku Kabushiki Kaisha) [15]. It presented a batch-wise procedure to produce spherical graphite particles, "using a vessel having a collision zone, in which jet air streams collide with each other, and a fluidizing zone". The influence of jet milling but also turbo-milling on the resulting shape of NG flakes in lab-scale was further reported by H. Wang et al. [16] in 1999, offering partially rounded, bent flakes. In 2000 M. Spahr et al. (Timcal) [17] applied for a patent in which again the rotational dry impact method was used in order to produce NG and SG powders with an increased bulk density (with an increase of 20–80%) and a high degree of roundness. The same method was employed by K. Ohzeki et al. [6,18] in order to produce partially rounded and also fully spherical NG particles in lab-scale. The spheroidization of SG materials in lab scale was furthermore described by C. Natarajan et al. [4] using a ball mill, and by Y.S. Wu et al. [19] utilizing "spheroidization machines" which were not further specified.

Normally, the quality of spherical graphite particles for LIBs is benchmarked with the help of physical characterization methods to determine the powder tap density, particle size distribution (PSD), particle shape, specific surface area, and the like, before the material is analyzed by time-consuming and cost-intensive electrochemical methods. However, none of the listed physical characterization methods provides information on the texture and internal (closed) porosity of the spherical particles, which undeniably are important quality criteria, as they influence the compactness and density of spheroidized particles. A high compactness and low porosity are favorable, as these materials will show a high density and high volumetric capacities in the electrode and cell. In contrast, a certain amount of porosity is considered beneficial to the long-term cycling stability, as the porosity allows absorbing parts of the volume increase of the graphite during lithiation [20].

It makes, furthermore, a difference, whether the porosity is constituted by open or by closed pores. In the case of open pores, the electrolyte may penetrate the interior of the particle, and the intercalation into the graphite phase may start from there, so that the overall lithiation process becomes faster. It is, however, well known, that the lithiation of graphite proceeds at potentials outside the electrochemical stability window of the electrolyte and that therefore the electrolyte is reductively decomposed, forming a passivation layer on the surface of the graphite. This layer is called "solid electrolyte interphase" (SEI). Its formation consumes charge and Li^+ and thus increases the irreversible capacity of the material. The higher the specific surface area of the material is, the higher is the irreversible capacity [21]. Due to the continuous SEI growth, the pores may finally be completely filled with SEI, and the beneficial effect of the open pores may gradually fade. Closed pores, instead, should show the beneficial effect of absorbing the volume increase, without additional SEI formation and irreversible capacity.

In 2010, Y.N. Jo et al. [22] reported a suitable method to study the texture of spherical graphite particles using scanning electron microscopy (SEM) coupled with focused ion beam (FIB) milling, by which cross section analysis of single particles is possible. This method gives a good first impression of the internal organization of the material but does not provide quantitative information about the internal porosity.

Very recently, S.M. Kwon et al. [23] have proposed isostatic pressing as a suitable method to increase the compactness and to reduce the internal porosity of spherical NG particles. The internal porosity of the particles was determined via mercury porosimetry, a method that normally reveals open porosity only, but gives no information about the closed porosity or texture of the particles.

In this work, we introduce an extended analysis method that enables the quantification of open and closed internal porosity and provides information about the complete texture of the particle. This method allows benchmarking the quality of spheroidized graphite materials in a more precise and complete way than it is possible with conventional physical characterization methods.

2. Experimental

2.1. Particle preparation

Highly crystalline NG flakes (purified; average flake diameter d_{50} = 250 μm; supplied by Graphit Kropfmühl GmbH) and bulky isostatic SG particles (particle diameter = 100–500 μm; provided by SGL Carbon GmbH) were used as starting materials.

These two types of graphite were mechanically spheroidized in lab-scale by means of a high speed rotational dry impact mill (Hybridizer, type NHS–0, Nara Machinery Co.). The general functionality of this device and the operating principle of the rotational dry impact method were described in detail in the literature before [12,13,18]. A schematic of the mill is shown in Fig. 1. In short, it works according to a rotor-stator principle in a batch-type mode. The system is equipped with a treatment chamber with a rotor and a recirculation duct. The rotor of 118 mm in diameter is fitted with six blades of 20 mm length and 5 mm thickness with flattened edges. During milling the particles can leave the treatment chamber via an outlet in the mantle and are re-fed into the chamber centre via the recirculation duct. The change in particle shape (from

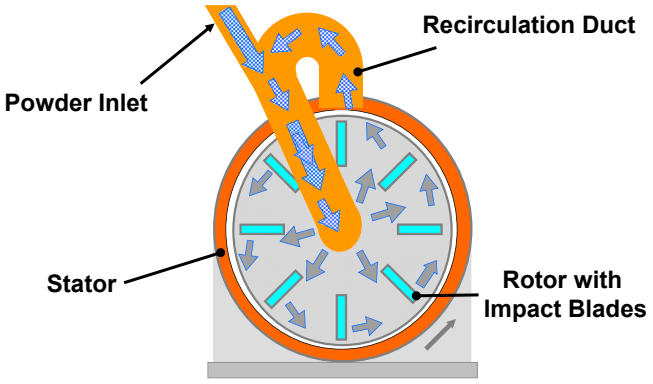

Fig. 1. Schematic of Hybridizer NHS-0 from Nara Machinery Co., including particle flow. (With kind permission of Nara Machinery Co.). (A colour version of this figure can be viewed online.)

flake to sphere) results from the repeated impacts of the flakes onto the rotor blades, onto the wall of the treatment chamber and onto other particles.

In order to evaluate the influence of the energy impact during spheroidisation on the resulting morphology and particle size of the investigated raw materials, 10 g batches of NG or SG were milled using either softer milling conditions ("medium impact", milling time = 240 s/rotation speed = 9000 rpm ≙ mill tip speed = 55.6 m/s, sample IDs: NG09 and SG07, respectively) or rougher milling conditions ("high impact", milling time = 480 s/rotation speed = 15,000 rpm ≙ mill tip speed 92.7 m/s, sample IDs: NG24 and SG18, respectively). All milled products were collected separately and carefully characterized with regard to their particle size and morphology by SEM imaging (LEO 1530 VP; LEO Elektronenmikroskopie GmbH/Zeiss) and PSD analysis (see below).

Subsequently, the milled/spheroidized samples were fractionated in order to confine their PSD to a range, which is comparable to that of commercially used anode materials. Two industrially manufactured spherical graphites served as reference: a NG material supplied by Graphit Kropfmühl GmbH (sample ID: NG_ref) and a SG material supplied by H.C. Carbon GmbH (sample ID: SG_ref).

The coarse fraction (particle size $\gg$40 μm) of the as-spheroidized samples was separated with an air jet sieve e200 LS (Hosokawa Alpine AG) using sieve inlets with mesh widths of 40, 32 or 20 μm, a sieving time of 5 min and a constant under-pressure of 2500 Pa. Ultra-fine particles (particle size $\ll$8 μm) as well as thin, flake-like particles were removed via air classification using a Picoline multi-process mill equipped with a Picosplit 20 ATP classifier module (Hosokawa Alpine AG). As classification parameter setup, a constant process air flow of 10 m^3/h and a rotation speed of the classifier wheel of initially 45,000 rpm and then 15,000 rpm were applied.

2.2. Particle characterization

Particle size distribution – The volume-based PSD was measured by laser diffraction with a Mastersizer Micro particle size analyzer (Malvern Instruments GmbH) using the basic mode (4OHD) with constant values for the particle refractive index (1.5295, 0.1000) and the dispersant refractive index (1.3300). For the measurements, the graphite powders were suspended in a solution of a surface-active agent (*Daxad 11*, sodium poly[(naphthaleneformaldehyde) sulfonate]) in distilled water by stirring and ultra-sonication. Following K. Ohzeki et al. [18] the median diameter d_{50} (corresponding to 50% undersize percentage) and a sharpness index d_{10}/d_{90} [= ratio of the particle diameters at 10% (d_{10}) and 90% (d_{90})], were defined to characterize the PSD.

Particle shape – Particle shape and size as well as the mean circularity of selected graphite materials were determined with a Sysmex FPIA-2100 image analysis system (Malvern Instruments GmbH), which is a flow cytometry-based analyzer. For the measurements, the graphite samples were suspended in distilled water (without surface-active agent) by sonication for 30 s.

Tap density – The tap density ρ_{2500} of graphite materials was determined by mechanically tapping approx. 5 mL of sample powder 2500 times with a STAV 2003 (J. Engelsmann AG) jolting volumeter and by dividing the mass of the sample powder through the compressed volume obtained after tapping.

2.3. SEM imaging, FIB, cross sections and porosity analysis

Sample preparation – All materials were powders. The conventional powder preparation on conductive carbon pads was not sufficient due to agglomeration of the particles and instability of the carbon pad beyond the ion beam. An improvement was obtained by using diluted silver glue from "Pelco® Colloidal Silver Liquid" and the matching "Gold/Silver Extender" from TED PELLA, INC. The silver glue was diluted in a 1:1 ratio to optimize the viscosity to obtain an adhesive thin film on top of the SEM pin stub. The sample powder was spread on the wet silver coating with a disposal brush. This method yields separated powder particles, which are conductively and solely fixed at the bottom part by the silver coating.

Data acquisition – SEM equipped with FIB technology enables to characterize the outside and inside morphology of materials in the nanometer range. The SEM/FIB studies were performed using the Zeiss Crossbeam NVision 40 Ar with the Gemini technology [24] and a Hitachi High-Tech SMI300 gallium ion source. For the SEM and FIB studies the powdered sample material was distributed as described above. The outer and inner morphology of the starting material and the rounded graphite were recorded with an accelerating voltage of 1 kV and an Everhart-Thornley detector (ETD) [25] to minimize charging effects. Firstly, cross-sections of half-sliced particles were produced [26] to study the inside morphology and texture. Therefore, a narrow platinum strip of approximately 1 μm thickness was sputtered with the gas injection system on the mid part of the selected particle to smoothen the rough surface and reduce curtaining effects. Then, for a rougher and faster milling, an accelerating voltage of 30 kV and currents between 13 up to 27 nA were selected. (The actual current depended on the selected particle size.) Further polishing was performed with an accelerating voltage of 30 kV with a stepwise decrease of current down to 700 pA. Due to the tilt of 54° to the optical axis, the resulting image distortion was corrected with the tilt correction of the SmartSEM software. The "Non-Local Means Denoising" [27,28] filter of ImageJ was applied to improve the signal to noise ratio.

In order to get insight into the particle volume, the particles were completely coated with a platinum layer deposited via the gas injection system. Trenches were milled on both sides and in front of the particle, for depositing the ablated carbon material. Then the sample was milled in thin slices, with 191 up to 478 slices per particle with a thickness between 53 and 157 nm, and corresponding SEM images were recorded using the ETD and an acceleration voltage of the electron beam of 1 kV. The alignment of the recorded image stack was performed with the "StackReg" [29] plugin of ImageJ. One of the crucial points for milling graphite particles is the high amount of re-deposition of milled material on the freshly cut cross-section. To counteract this problem, trenches were milled as deep as the height of the particle (about 10 μm–17 μm) on both sides and in front of the particle for depositing the milled graphite. The depths of the FIB cuts were set accordingly. This prevented unwanted re-deposition, but increased strongly the time for recording the tomogram.

Furthermore, the particle nature of the samples caused another issue. The samples were intentionally prepared in such a way that the particles did not sink into the silver glue, which enabled to examine the whole surface and the general appearance. It was, especially for FIB tomograms, a major factor not to miss any parts of the particle that were buried under the silver glue. This kind of sample preparation led to tilting or even falling over, when the larger part of the particle was milled away. This issue was solved by depositing an additional thick layer of platinum on the rear part of the particle, acting as a support.

The errors of the FIB tomograms were estimated by manually dilating and eroding single pixels of the areas of interest in the two dimensional image data and repeating the data evaluation [30].

3. Results and discussion

Six spheroidized graphite materials have been investigated in

this study. These include two NGs obtained from purified flake graphite and two SGs obtained from isostatic graphite, using rotational dry impact blending with two different sets of process parameters (with medium and high energy impact). A commercial spheroidized NG and a commercial spheroidized SG serve as reference materials.

It should be mentioned, that the isostatic graphite material under investigation is not a perfect candidate for a LIB anode material, since it displays a lower graphitization degree and thus a lower Li intercalation capacity (of around 290 mAh/g) than what is usually found (330–365 mAh/g). It has been selected deliberately here for its smaller crystallite size and higher hardness as opposed to the soft and highly crystalline NG. This allows studying the effects of the mentioned raw material properties on the spheroidization process and on the structure, texture and morphology of the spheroidized products.

3.1. Particle size and shape

The materials obtained during the spheroidization/milling process have very broad PSDs and contain spherical particles in the target particle size range of 8–30 μm (for applications as anode material in LIBs), but also larger particles, which are mainly unspheroidized, and smaller particles, which are both spheroidized and unspheroidized. To separate the target material, it has been fractionated by sieving and classifying as described in the Experimental section. To be able to directly compare the different materials, identical sieving and classification parameters have been applied to all four materials. The milling/spheroidization conditions of the prepared graphite samples (NG09, NG24, SG07 and SG18) and their properties, collected directly after the spheroidization/milling treatment (_milled) and after additional fractionation (_milled + fractionated), are summarized in Table 1. The properties of the reference materials (NG_ref and SG_ref) are given for comparison.

With increasing energy impact during the spheroidization process, the size of the resulting NG and SG particles decreases significantly, the aspect ratio decreases and the particles become more spherical in shape. This correlation has been described before [6]. Thus, NG flakes, which have been spheroidized with medium milling impact (NG09; velocity = 9000 rpm/milling time = 240 s) provide a d_{50} value of 19.6 μm, while NG flakes milled with a significantly higher energy impact (NG24; 15,000 rpm/480 s) offer a ~70% smaller d_{50} value of only 6.1 μm. A similar trend is observed for the SG raw material (SG), as the high energy impact during spheroidization (SG18; 15,000 rpm/480 s; d_{50} = 4.0 μm) generates a ~55% smaller d_{50} value as obtained using the medium impact (NG07; 9000 rpm/240 s; d_{50} = 8.7 μm).

All as-milled samples display a sharpness index d_{10}/d_{90} of around 0.05, indicating very broad PSDs, as shown in Fig. 2a. Such broad PSDs are typical of batch-type milling processes.

Large particles with diameters ≫30 μm imply an incomplete spheroidization process, due to too short milling times. When used as anode material for LIBs, these big particles would have an adverse influence on the electrode preparation process, resulting in an inhomogeneous electrode slurry and a poor adhesion of the graphite coating on the current collector. In contrast, a high amount of small particles with a diameter ≪8 μm indicates too high a milling impact causing an extensive breaking-off of the corners and edges of the NG flakes. Because of their small size and irregular shape, the fine particles introduce a high specific surface area, which increases the irreversible capacity and lowers the attainable electrode density. Both the fine and the coarse by-products decrease the yield of spherical graphite particles with the desired particle size. The big flakes of coarse by-product can, in principle, be re-fed into the spheroidisation process, thus increasing the yield. Too small particles are lost in this regard and should be avoided during processing.

For the NGs, the medium impact milled sample NG09 offers a yield of 51% of particles with an appropriate size (calculated from the volume-based PSD), whereas the high impact milled sample NG24 offers a yield of 22%. For the SGs, the medium impact milled sample SG07 offers a yield of 40% and the high impact milled sample SG18 a yield of 27%. Thus, increasing the energy impact during spheroidisation promotes an actual milling with a decrease of particle size in addition to spheroidisation, and thus reduces the yield of particles which can be used for LIBs.

All milled samples were fractionated in order to remove too big and too small particles. The resulting PSDs of the main fractions are shown in Fig. 2b. The particle shape analysis provides a mean circularity of ≥0.9 for all milled and fractionated samples, indicating a high degree of roundness. Regarding the ratio of particles with a size in a range of 5–10 μm to those in the range of 10–40 μm of fractionated samples, both medium impact milled samples (NG09 and SG07) offer a high amount of particles bigger than 10 μm (72% and 81%, respectively), while the high impact milled samples NG24 and SG18 feature more than 80% of particles smaller than 10 μm.

The medium impact NG sample NG09 (milled and fractionated) shows similar values for the sharpness index (~0.5), tap density (>0.9 g/cm^3) and mean circularity (>0.9), as the NG reference material. Hence, for the NG raw material under investigation, a spheroidisation treatment with 9000 rpm for 240 s seems to be the best one to reproduce the commercial reference material.

Table 1
Overview of spheroidization/milling conditions and results of volume-based particle size distribution, tap density and particle shape analysis of the prepared samples and reference materials.

	Milling conditions		d_{10} [μm]	d_{50} [μm]	d_{90} [μm]	d_{10}/d_{90}	Tap density ρ_{2500} [g/cm^3]	Mean circularity	% of total counts for particles (number-based)	
	Time [s]	Speed [rpm]							Particle size 5–10 μm	Particle size 10–40 μm
NG_ref	–	–	7.5	10.5	15.1	0.50	0.92	0.93	58.0	42.0
NG09_milled	240	9000	5.3	19.6	107.5	0.05	–	–	–	–
NG09_milled + fractionated	240	9000	16.6	22.2	30.7	0.54	0.99	0.95	27.9	72.1
NG24_milled	480	15,000	2.1	6.1	77.4	0.03	–	–	–	–
NG24_milled + fractionated	480	15,000	15.0	26.6	48.5	0.31	–	0.94	85.0	15.0
SG_ref	–	–	10.3	18.6	32.8	0.31	0.85	0.90	23.6	76.4
SG07_milled	240	9000	2.1	8.7	46.7	0.04	–	–	–	–
SG07_milled + fractionated	240	9000	17.1	26.4	41.1	0.42	1.15	0.97	19.4	80.7
SG18_milled	480	15,000	1.1	4.0	19.0	0.06	–	–	–	–
SG18_milled + fractionated	480	15,000	14.6	24.6	39.4	0.37	–	0.94	81.7	18.3

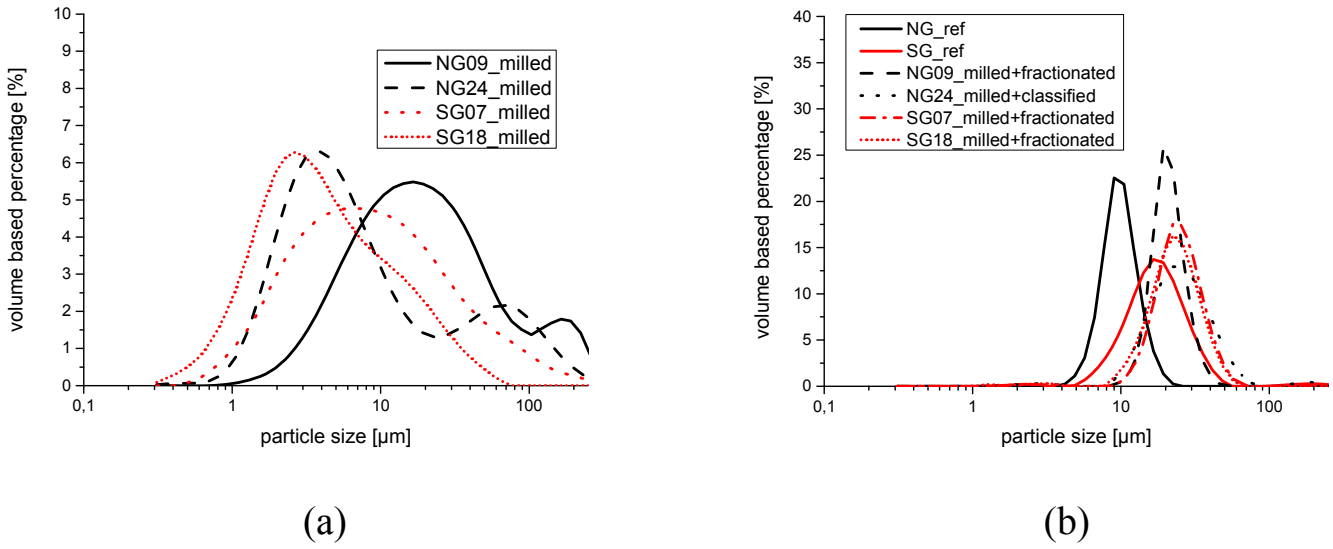

Fig. 2. Particle size distributions of (a) spheroidized/milled graphite samples and (b) spheroidized/milled plus fractionated graphite samples, including the reference materials.

The SG reference material has a lower sharpness index and a lower tap density than all the other materials. The medium impact SG sample SG07 has a higher sharpness index than the synthetic reference material but a smaller one than the NG samples. It has the highest tap density, which, beside particle size and shape, is related with the bulky and unporous nature of the raw material (isostatic graphite).

Interestingly, the sharpness index is lower for the high impact milled and fractionated samples than for the medium impact milled ones, although the sieving and classifying conditions are similar in both cases. This is mainly related to the fact that for the medium impact samples the maximum of the PSD of the fractionated samples is closer to that of the unfractionated samples. Therefore, the fractionation process selects that portion of the unfractionated

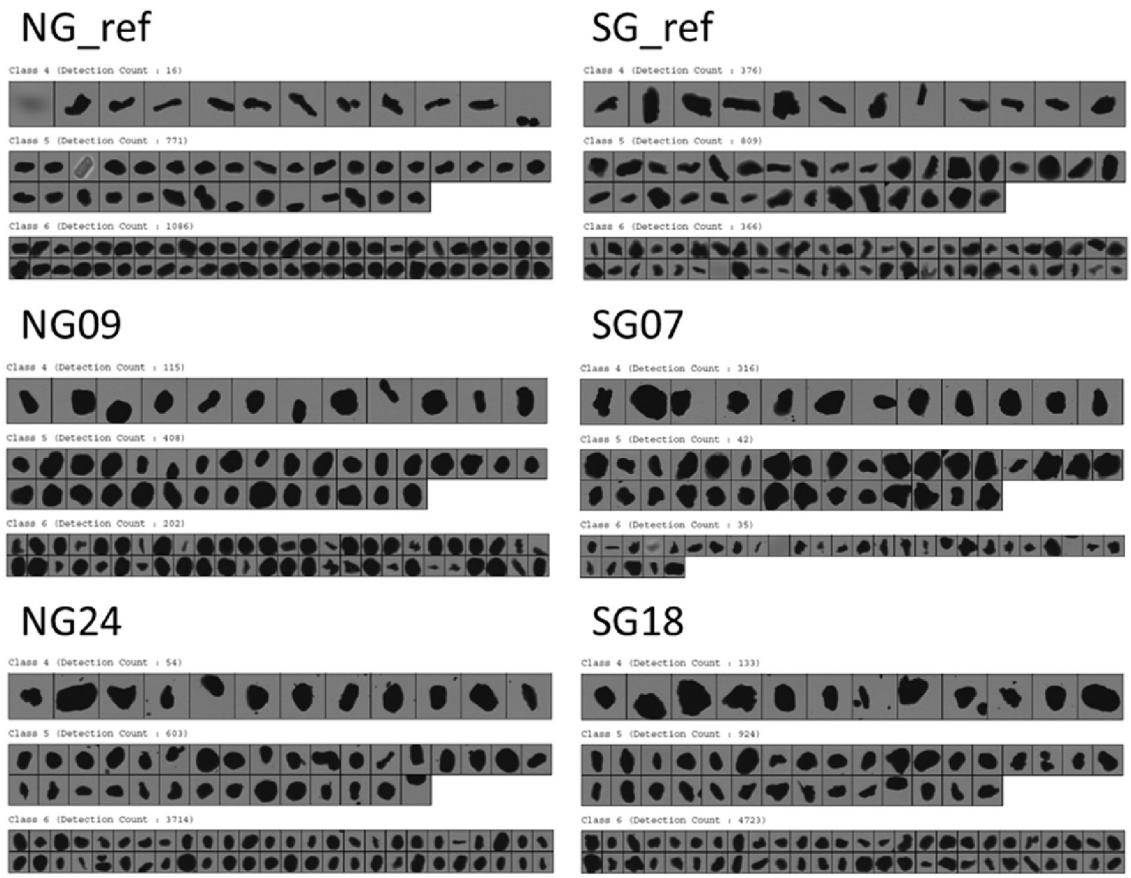

Fig. 3. Particle shape analysis of spheroidized and fractionated graphite samples and reference materials (class 4: 20–40 µm, class 5: 10–20 µm, class 6: 5–10 µm).

samples which includes the maximum of the PSD, resulting in a steep PSD of the fractionated material. For the high impact samples, the maxima are further apart and the fractionated sample is extracted from the upper tail of the PSD of the original material, resulting in a flatter PSD of the fractionated sample. In order to obtain a maximum spheroidization yield with a narrow PSD the spheroidisation and fractionation processes should be adjusted to each other and to the target PSD.

Fig. 3 provides an optical comparison of the morphological profile of spheroidized and fractionated samples and reference materials. Therefore, particles of different sizes have been arranged into several size classes (class 4: 20–40 μm, class 5: 10–20 μm and class 6: 5–10 μm) and quantified by the number of particle counts.

NG_ref features mostly uniformly shaped, spherical particles of class 6 (1086 counts) and rather oval-shaped particles of class 5 (771 counts). In addition, there is a limited set of particles of class 4 having an elongated shape (16 counts). In comparison, the medium impact milled and fractionated NG sample NG09 offers spherically shaped particles in all listed classes – an indication for a successful extensive spheroidization. Furthermore, particles with elongated shape are detected in class 4 and 6, but hardly in class 5. The largest number of counts was achieved for class 5 particles (408) followed by class 6 (202) and class 4 particles (115). For the high impact milled and fractionated NG sample NG24, class 6 particles constitute the largest portion in terms of particle counts (3,714), which is in line with the observed reduction of the average particle size. The class 6 particles show a high degree of roundness. But also the shape of particles of size class 5 (403 counts) and 4 (54 counts) is considered to be rather spherical than flake-like or elongated.

The situation is somewhat different for the SG reference. It is

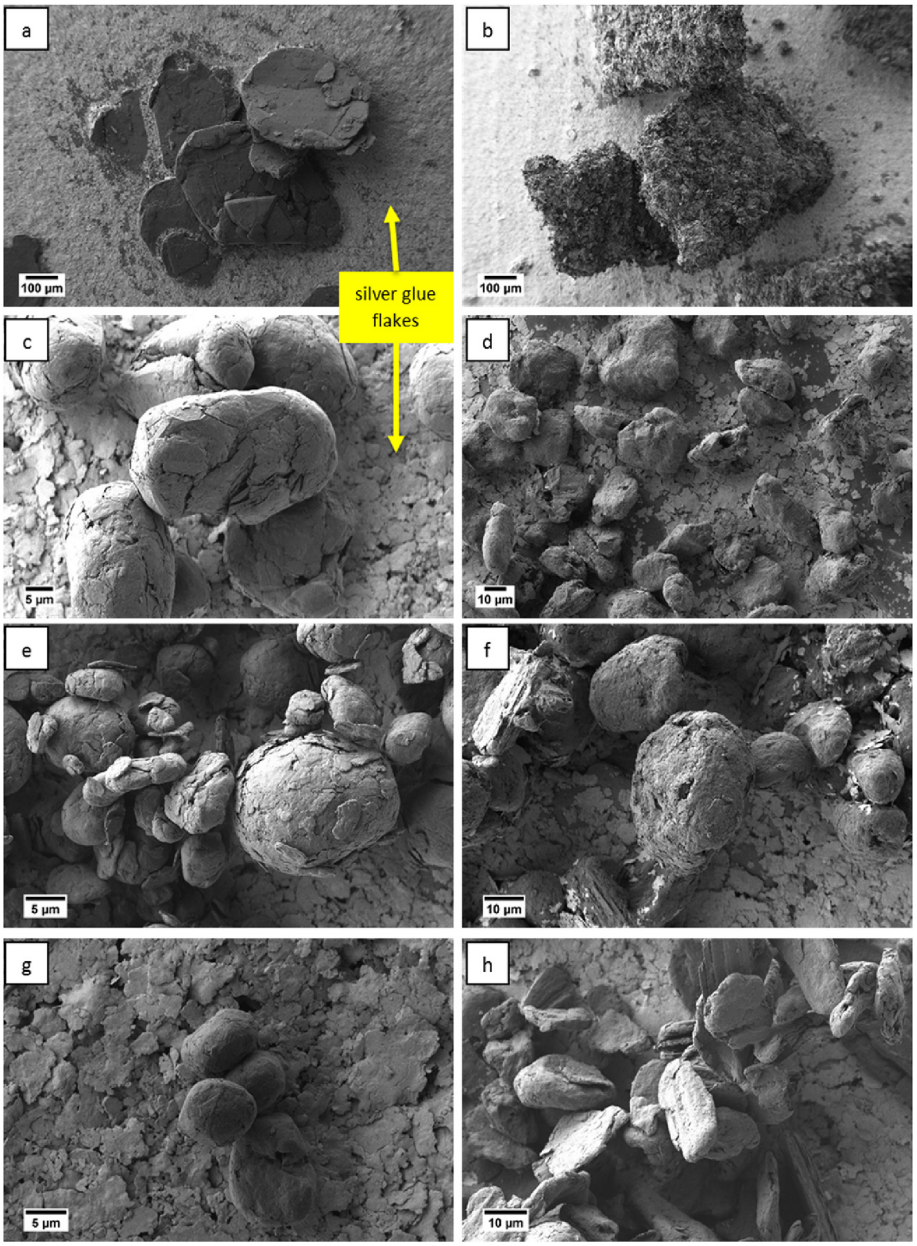

Fig. 4. SEM images of natural (left column) and synthetic (right column) graphite particles before and after milling. (a) and (b) raw materials before milling, (c)–(f) after milling: (c) and (d) with 9000 rpm for 240 s (NG09, SG07), (e) and (f) with 15,000 rpm for 480 s (NG24, SG18), (g) and (h) reference samples (NG_ref, SG_ref). (A colour version of this figure can be viewed online.)

less spherical (mean circularity = 0.85) than the NG reference (mean circularity = 0.92), and the particles of all size classes seem to be rarely spherical but rather elongated, flat and irregularly shaped, with rough surfaces. The ratio of particle counts of size classes 4: 5: 6 is 376: 809: 366. For the medium impact milled SG sample SG07, particles with more spherical shapes were detected, compared to the synthetic reference material. This can again be interpreted as an indication for successful spheroidization in lab-scale, even if the shape is less spherical than it is for the NG materials. SG07 is mainly composed of particles in the range of 20–40 μm (class 4: 316 counts, class 5: 42 counts and class 6: 35 counts).

The high impact milled SG sample SG18 offers a similar composition as the high impact milled NG sample NG24. The most extensive amount of particle counts is found for particle size class 6 (4723) followed by classes 5 (924) and 4 (133). The overall shape of the particles is more spherical than the one of the SG reference and medium impact milled SG sample, but generally less uniform than the shape of the spheroidized NG materials.

3.2. Morphology and texture

The outward morphology of the particles, both of the NGs and the SGs, was imaged using SEM, as shown in Fig. 4. The NG starting material (Fig. 4a) has a flake-like appearance, whereas the SG starting material (Fig. 4b) is more orthogonal. The SG shows a much rougher surface topography. The outward morphology of the material changes significantly after the spheroidization/milling process. All batches presented in Fig. 4c–f show rounded particles. Whereas the NG materials have a rather spherical or at least potato-

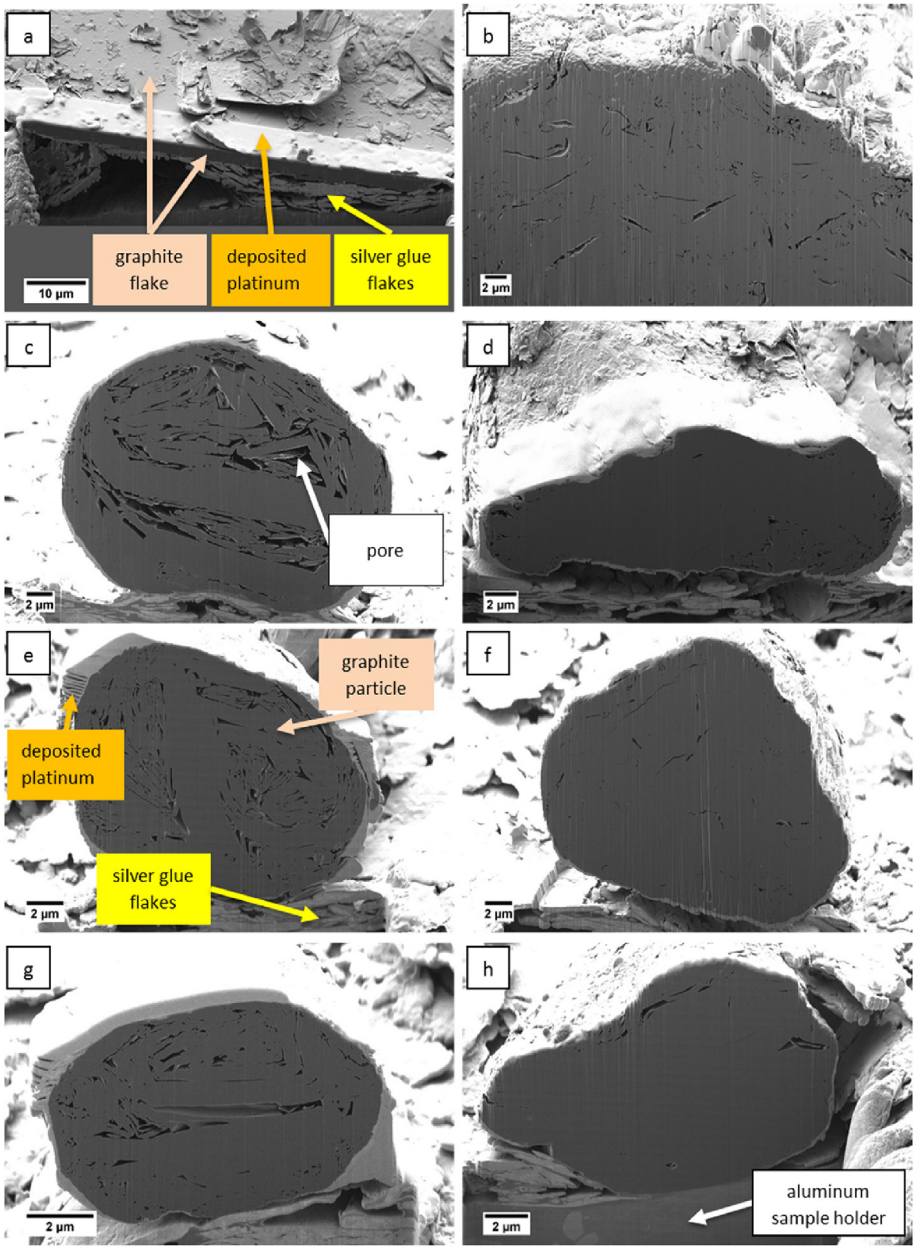

Fig. 5. FIB cross-sections of natural (left column) and synthetic (right column) graphite at different milling conditions. (a), (b) starting materials before milling, (c)–(f) materials after milling: (c) and (d) with 9000 rpm for 240 s (NG09, SG07), (e) and (f) with 15,000 rpm for 480 s (NG24, SG18), (g) and (h) reference samples (NG_ref, SG_ref). (A colour version of this figure can be viewed online.)

like shape, the SG materials have more irregular, angular shapes. For the NG materials smaller flakes can be distinguished on the surface, which most likely stem from a re-attachment of graphite fragments onto the surface of bigger spherical particles.

The FIB cross-sections of Fig. 5 give insight to the inner morphology and texture. Fig. 5a depicts the cross section of a single flake of the NG raw material. This material contains almost no pores. The cross sections in Fig. 5c, e and g were prepared from spheroidized NGs. They show folded graphite flakes, where the structure of the original graphite flakes is still partially visible, leaving unfilled areas in between. The unfilled areas show mostly elongated shapes in one direction, forming slit-shaped pores. With increasing energy impact during spheroidization/milling the porosity decreases (compare Fig. 5c and e). The self-spheroidized samples show a similar texture as the commercial reference NG reference (Fig. 5g). Overall, the spheroidization of NG resulted in the formation of a significant amount of pores, which were not present in the raw material.

The cross section in Fig. 5b reveals the inner build of the SG raw material, and those in Fig. 5d, f and h the inner build of the rounded SGs. It is seen that this type of isostatic SG contains some amount of porosity (unlike the NG flakes). The spheroidization does not have a significant impact on this porosity. This is ascribed to the higher hardness of the isostatic SG. Furthermore, the material is more isotropic in appearance than the strongly anisotropic NG material composed of flakes. Therefore, the folding and bending mechanism, which occurs for NG and which induces slit-shaped pores, is absent in the SG material under investigation. Compared to the spheroidized NGs, the rounded SGs show a significantly higher density and smaller porosity. Also the SG reference material, which shows a higher capacity (of around 330 mAh/g) and higher graphitization degree than the self-spheroidized SG materials, is rather compact and exhibits only a small amount of porosity.

The unfilled regions can be divided into two classes of pores, closed and open ones. Closed pores have no connection to the particle surface and stay unfilled. They are considered as dead volume, which is not available for intercalation processes and decreases the volumetric energy density of the lithium ion battery. On the positive side, they may improve the long-term cycling stability, as discussed in the Introduction section. Open pores have a connection to the particle surface and could be filled up with liquid electrolyte during cycling. They contribute to the particle surface and increase the SEI layer formation, causing an increase of the irreversible capacity. The open and closed porosity can be calculated quantitatively by the equation [31]:

$$\Phi_{O,C} = \frac{V_{O,C}}{V} \cdot 100,$$

where Φ_O is the open and Φ_C the closed porosity in %, V is the volume of the whole particle including pores, and V_O, V_C are the volumes of the open and closed pores, respectively.

FIB tomography was utilised to investigate the porosity quantitatively. Fig. 6 shows representations of fully segmented three-dimensional FIB tomograms of a single graphite flake from the NG starting material (Fig. 6a), a particle of NG spheroidized at

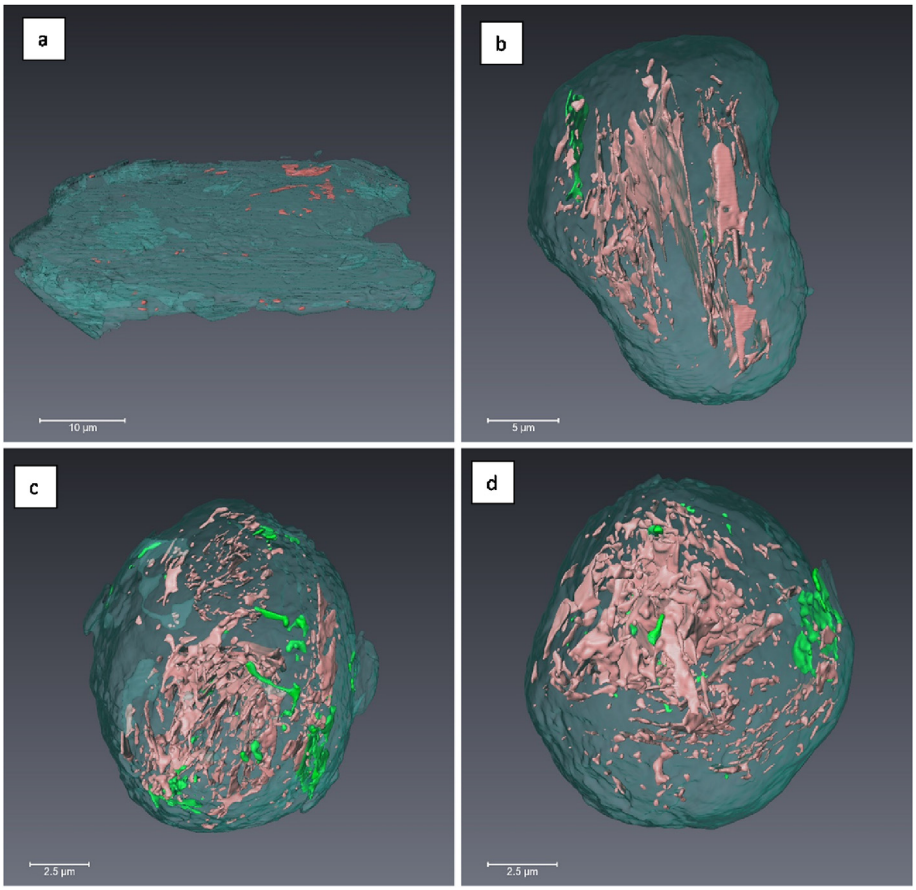

Fig. 6. FIB tomograms of natural graphite obtained at different spheroidization conditions: (a) raw material before milling, (b) material from spheroidization with 9000 rpm for 240 s (NG09), (c) material from spheroidization with 15,000 rpm for 480 s (NG24), (d) commercial reference material (NG_ref). Open pores are shown in green and closed pores in red.

Table 2
Particle volume and total, closed and open porosity for the NG starting material and for the self-spheroidized and commercial reference NGs.

	NG starting material	NG09	NG24	Commercial NG reference
Total volume (μm^3)	3160 ± 6	4444 ± 178	853 ± 34	666 ± 27
Total porosity (%)	0.8 ± 0.5	5.1 ± 2.2	4.5 ± 2.5	4.9 ± 2.1
Closed porosity (%)	–	5.0 ± 2.2	4.0 ± 2.3	4.5 ± 2.0
Open porosity (%)	–	0.1 ± 0.05	0.5 ± 0.2	0.4 ± 0.2
Milling time (s)	–	240	480	–
Milling speed (rpm)	–	9000	15,000	–

medium impact conditions (Fig. 6b) and a particle of NG spheroidized at high impact conditions (Fig. 6c). A three-dimensional FIB tomogram of the commercial spheroidized graphite is included for comparison (Fig. 6d).

Table 2 presents the determined particle volumes and the open and closed porosities for all four tomograms. The spherical graphites yield total porosities in the range of 4.5 ± 2.5% to 5.1 ± 2.2%, closed porosities in the range of 4.0 ± 2.3% to 5.0 ± 2.2% with lower values for the higher milling impact force, and open porosities in the range of 0.1 ± 0.05% to 0.5 ± 0.2% with higher values for the higher milling impact force. The investigated flake from the NG starting material has a comparably low porosity with 0.8%, whereby a distinction between open and closed porosity was not made because the errors would be unreasonably high. The results indicate that high impact treatment leads to a higher compression decreasing the closed porosity, and produces additional cracks and/or picking up of small fragments increasing the open porosity. The porosities of the reference sample are in between those of the two self-spheroidized materials.

4. Conclusions

The spheroidization of NG by rotational impact blending involves several phenomena: Large flakes are folded and bent, and frequently act as the core backbone of the spherical particles. Edges of large flakes are broken off, resulting in a milling effect. Generally, the particle size decreases as the energy impact during the spheroidization procedure increases. Furthermore, smaller graphite fragments are (re-)attached to the spherical graphite particles. All these mechanisms transform the more or less unporous graphite flakes into spherical materials, which contain a significant amount of porosity, in the range of 4–5% of closed pores and of up to 0.5% of open pores (referred to the total particle volume). An increase in the energy impact during the spheroidization process increases the open porosity and decreases the closed porosity. This will influence the electrochemical properties when used as anode material for LIBs, which will be discussed in detail in a forthcoming paper.

The situation is different for the hard and compact isostatic SG. Here the spheroidization process results in a milling effect as well. But the overall shape is less spherical than for the NG, and one obtains rather angular materials with rounded edges. Furthermore, the spheroidization results in a significant smoothing of the surface. The porosity does not change significantly during spheroidization.

FIB-SEM cross-sections and tomography have been shown to yield detailed and quantitative information on the internal morphology and texture of the graphite particles. A lot of effort has been put into the development of a suitable and reliable sample preparation method and into the optimization of the analysis parameters. Tomography allows especially to quantify the internal porosity of the spherical particles, which at contrary to the open porosity is not easily measurable by other, conventional methods. This information helps to better understand the spheroidization process and to link the electrochemical performance to the underlying material properties.

Acknowledgements

The authors are indebted to the German Federal Ministry of Education and Research (BMBF) for funding this work in the project "LiEcoSafe" (contracts no. 03X4636A/C). They are, furthermore, grateful to Graphit Kropfmühl GmbH, SGL Carbon GmbH and H.C. Carbon GmbH for providing raw materials and reference materials.

References

[1] C. Pillot, The rechargeable battery market and main trends 2014 – 2025, in: AABC Europe 2016 – Advanced Automotive Battery Conference; Mainz, Germany, 2016.
[2] European Commission: Report on Critical Raw Materials for the EU, 2014.
[3] C. Frey, Verwendung von Naturgraphit in Lithium-Ionen-Akkus – Auslöser eines Explorationsbooms, in: Spring Meeting of the German Carbon Group; Meitingen, Germany, 2016.
[4] C. Natarajan, H. Fujimoto, A. Mabuchi, K. Tokumitsu, T. Kasuh, Effect of mechanical milling of graphite powder on lithium intercalation properties, J. Power Sources 92 (2001) 187–192.
[5] Y. Ishii, A. Fujita, T. Nishida, K. Yamada, High-performance anode material for lithium-ion rechargeable battery, Hitachi Chem. Tech. Rep. 36 (2001) 27.
[6] K. Ohzeki, Y. Saito, B. Golman, K. Shinohara, Shape modification of graphite particles by rotational impact blending, Carbon 43 (2005) 1673–1679.
[7] F. Disma, L. Aymard, L. Dupont, J.M. Tarascon, Effect of mechanical grinding on the lithium intercalation process in graphites and soft carbons, J. Electrochem. Soc. 72 (1) (1996) 3959–3971.
[8] F. Salver-Disma, J.M. Tarascon, C. Clinard, J.N. Rouzaud, Transmission electron microscopy studies on carbon materials prepared by mechanical milling, Carbon 37 (1999) 1941–1959.
[9] These values are based on datasheets of commercially available anode materials and on tear-down analyses of commercial Li-ion cells in our laboratories.
[10] K. Seino, B. Golman, K. Shinohara, K. Ohzeki, Variation of packing structure of cast film with preparation conditions and particle properties, Tanso 216 (2005) 2–7.
[11] K. Ohzeki, Y. Ohsaki, B. Golman, K. Shinohara, Influence of void-size distribution of anode film made of natural graphite particles on high rate discharge capability of lithium-ion battery, Tanso 213 (2004) 140–143.
[12] M. Otani, T. Uchiyama, H. Minoshima, K. Shinohara, K. Takayashiki, N. Nakao, Factors on particle shape control by dry impact blending method, Int. J. Soc. Mater. Eng. Resour. 7 (1994) 35–45.
[13] M. Otani, H. Minoshima, T. Ura, K. Shinohara, Mechanism of particle shape modification by dry impact blending, Adv. Powder Technol. 7 (4) (1996) 291–303.
[14] F. Honda, H. Honda, M. Koishi, Utilization of the dry impact blending method to prepare irregularly shaped particles for high-performance liquid chromatographic column packings, J. Chromatogr. A 696 (1995) 19–30.
[15] S. Kubota, Modified graphite particles derived from scaly natural ones, production thereof and secondary battery, CA 2246953 C, 2001.
[16] H. Wang, T. Ikeda, K. Fukuda, M. Yoshio, Effect of milling on the electrochemical performance of natural graphite as an anode material for lithium-ion battery, J. Power Sources 83 (1999) 141–147.
[17] M.E. Spahr, Verfahren zur Herstellung von Graphitpulvern mit erhöhter Schüttdichte, EP 1240103 B1, 2007.
[18] K. Ohzeki, K. Seino, T. Kumagai, B. Golman, K. Shinohara, Characterization of packing structure of tape cast with non-spherical natural graphite particles, Carbon 44 (2006) 578–586.
[19] Y.S. Wu, T.S. Yeh, Y.H. Lee, Y.C. Lee, Spheroidization Modification of artificial graphite applied as anode materials for high rate lithium ion batteries, Adv. Mater. Res. 201–203 (2011) 421–424.
[20] Y. Ishii, T. Nishida, A. Fujita and K. Yamada, Graphite particles and lithium secondary cell using them as cathode material, WO9806679, 1998.
[21] F. Joho, B. Rykart, A. Blome, P. Novàk, H. Wilhelm, M.E. Spahr, Relation between surface properties, pore structure and first-cycle charge loss of graphite as negative electrode in lithium-ion batteries, J. Power Sources 97–98 (2001) 78–82.
[22] Y.N. Jo, Y. Kim, J.S. Kim, J.H. Song, K.J. Kim, C.Y. Kwag, et al., Si–graphite

composites as anode materials for lithium secondary batteries, J. Power Sources 195 (2010) 6031–6036.
[23] S.M. Kwon, Negative electrode active material for rechargeable lithium battery, method for preparing the same and rechargeable lithium battery using the same, US 20150155557 A1, 2015.
[24] E.L. Principe, P. Gnauck, P.A. Hoffrogge, Three beam approach to TEM preparation using in-situ low voltage argon ion final milling in a FIB-SEM instrument, Microsc. Microanal. 11 (Suppl.02) (2005) 830–831, http://dx.doi.org/10.1017/S1431927605502460.
[25] L. Reimer, U. Golla, R. Böngeler, M. Kässens, B. Schindler, R. Senkel, Charging of bulk specimens, insulating layers and free-supporting films in scanning electron microscopy, Optik 92 (1992) 14–22.
[26] C.A. Volkert, A.M. Minor, Focused ion beam microscopy and micromachining, MRS Bull. 32 (2007) 389–399, http://dx.doi.org/10.1557/mrs2007.62.
[27] A. Buades, B. Coll, J.-M. Morel, A non-local algorithm for image denoising, in: Computer Society Conference on Computer Vision and Pattern Recognition, vol. 2, 2005, pp. 60–65.
[28] J. Darbon, Fast nonlocal filtering applied to electron cryomicroscopy, in: 5th IEEE International Symposium on Biomedical Imaging: from Nano to Macro, Proceedings, ISBI, IEEE, 2008, pp. 1331–1334.
[29] P. Thevenaz, U.E. Ruttimann, U. Unser, A pyramid approach to subpixel registration based on intensity, IEEE Trans. Image Process. 7 (1) (1998) 27–41.
[30] A.V. Nagasekhar, C.H. Caceres, C. Kong, 3D characterization of intermetallics in a high pressure die cast Mg alloy using focused ion beam tomography, Mater. Charact. 61 (2010) 1035–1042.
[31] J.H. Schön, Physical Properties of Rocks, Oxford Elsevier, 2011, p. 18.